Eur Biophys J (2010) 39:307–325
DOI 10.1007/s00249-009-0548-4

ORIGINAL PAPER

Structural and dynamic properties of juxta-membrane segments of caveolin-1 and caveolin-2 at the membrane interface

Charlotte Le Lan · Jacques Gallay · Michel Vincent · Jean Michel Neumann · Béatrice de Foresta · Nadège Jamin

Received: 19 May 2009 / Revised: 15 September 2009 / Accepted: 24 September 2009 / Published online: 22 October 2009

Abstract Caveolins (cav1–3) are essential membrane proteins found in caveolae. The caveolin scaffolding domain of cav-1 includes a short sequence containing a CRAC motif (V94TKYWFYR101) at its C-terminal end. To investigate the role of this motif in the caveolin–membrane interaction at the atomic level, we performed a detailed structural and dynamics characterization of a cav-1(V94-L102) nonapeptide encompassing this motif and including the first residue of cav-1 hydrophobic domain (L102), in dodecylmaltoside (DM) or dodecylphosphocholine (DPC) micelles, as membrane mimics. Cav-1(V94-L102) partitioned better in DPC and in DM/anionic lipid micelles than in DM micelles, as shown by fluorescence titration and CD. NMR data revealed that this peptide folded as an amphipathic helix located in the polar head group region of DPC micelles. The two tyrosine side-chains, flanked by arginine and lysine residues, are situated on one face of this helix, whereas the phenylalanine and tryptophan side-chains are located on the opposite face. Fluorescence studies showed significant Trp subnanosecond rotations, the presence of several rotamers, and a heterogeneous location within the water/micelle interface. NMR studies of the shorter cav-1(V94-R101) peptide and of the homologous sequence of cav-2(I79SKYVMYKF87) allowed the description of the effect of L102 and of the amino acid variations occurring in cav-2 on the structure and localization in DPC micelles. Based on the topological model of caveolins, our results suggest that the cav-1 and cav-2 nonapeptides studied form interfacial α-helix membrane anchors in which the K/RhhhYK/Rh motif, also found in cav-3, may play a significant role.

Keywords Caveolin · Interface · Fluorescence · NMR · DPC · DM

Abbreviations

BrDM	7,8-Dibromododecylmaltoside
BrUM	10,11-Dibromoundecanoylmaltoside
cmc	Critical micellar concentration
CD	Circular dichroism
CRAC	Cholesterol recognition/interaction amino acid consensus
cav-*n*	Caveolin-*n* with $n = 1$, 2 or 3
DM	*n*-Dodecyl-β-D-maltoside
DMPA	1,2-Dimyristoyl-sn-glycero-3-phosphate
DMPC	1,2-Dimyristoyl-sn-glycero-3-phosphocholine
DMPG	1,2-Dimyristoyl-sn-glycero-3-[phospho-rac-(1-glycerol)]
DMPS	1,2-Dimyristoyl-sn-glycero-3-phospho-L-serine
DPC	Dodecylphosphocholine
DSS	Dimethylsilapentane-sulfonic acid
FWHM	Full width at half maximum

Electronic supplementary material The online version of this article (doi:10.1007/s00249-009-0548-4) contains supplementary material, which is available to authorized users.

C. Le Lan · J. M. Neumann · B. de Foresta · N. Jamin (✉)
CEA, iBiTecs, SB2SM, 91191 Gif-sur-Yvette, France
e-mail: nadege.jamin@cea.fr

C. Le Lan · J. M. Neumann · B. de Foresta · N. Jamin
CNRS, URA 2096, 91191 Gif-sur-Yvette, France

J. Gallay · M. Vincent
Institut de Biochimie et de Biophysique Moléculaire et Cellulaire, Université Paris-Sud, UMR8619-CNRS, IFR115, 91405 Orsay, France

HSQC	Heteronuclear single quantum correlated spectroscopy
MALDI/TOF	Matrix-assisted laser desorption ionization time of flight
MEM	Maximum entropy method
N-MAD	N-terminal membrane attachment domain
NATA	*N*-acetyltryptophanamide
NOESY	Nuclear Overhauser effect spectroscopy
POPC	1-Palmitoyl-2-oleoyl-*sn*-glycero-3-phosphocholine
POPS	1-Palmitoyl-2-oleoyl-*sn*-glycero-3-[phospho-L-serine]
POPG	1-Palmitoyl-2-oleoyl-*sn*-glycero-3-[phospho-*rac*-(1-glycerol)]
TOCSY	Total correlated spectroscopy

Introduction

Caveolins (1–3) are major protein components of caveolae, microdomains of the plasma membrane involved in a large number of biological functions, including signal transduction, cholesterol homeostasis, and transport (Cohen et al. 2004; Parton and Simons 2007 and references therein). Caveolin-1 and caveolin-2 (cav-1 and cav-2) are found in most cell types, including adipocytes, small muscle cells, endothelial cells, epithelial cells, and fibroblasts, whereas caveolin-3 (cav-3) is specific to muscle. Cav-1 and cav-3 can form invaginated caveolae independently, whereas cav-2 requires colocalization with cav-1. There are many lines of evidence to suggest that caveolins are not only structural elements of caveolae but also interact with signaling proteins transiently sequestered in these microdomains, modulating their activity (Liu et al. 2002). Essential interaction networks involving sterols, lipids, and proteins clearly exist within caveolae, and investigations of their molecular basis are required to understand the structure and multifunctional role of these membrane microdomains.

A series of biochemical studies have led to a consensus topological model for cav-1, the best characterized member of the caveolin protein family. This model comprises a hydrophobic intramembrane domain, L102-I134, flanked at its N- and C-termini by two amphipathic cytosolic segments: D82-R101 and K135-I150 (Cohen et al. 2004; Parton et al. 2006 and references therein). The two amphipathic regions probably constitute in-plane membrane anchors, known as N- and C- attachment domains (N-MAD and C-MAD, respectively; Cohen et al. 2004; Schlegel et al. 1999). N-MAD, which is also known as the caveolin scaffolding domain, has been identified as an essential element for the interaction between caveolin and proteins involved in signal transduction (Schlegel et al. 1999). The amino acid sequences of cav-1 and cav-3 are very similar and differ slightly from that of cav-2: the human cav-1 and cav-3 sequences are about 85% similar, whereas the human cav-1 and cav-2 sequences are about 58% similar. However, the level of similarity between the human cav-1 and cav-2 sequences is as high as 73% for the corresponding central intramembrane domains (R-L102-I134-K in cav-1 and K-F87-V119-K in cav-2).

Ten years ago, Li and Papadopoulos noticed that the C-terminal sequence of the cav-1 N-MAD, V94-T-K-Y-W-F-Y-R101 (Fig. 1), matched the cholesterol recognition/interaction amino acid consensus (CRAC) pattern [i.e. *V/L*−*X*(1–5)–*Y*−*X*(1–5)−*R/K*, where *X*(1–5) represents from one to five residues of any amino acid], highlighting a possible role for this sequence in the binding of the protein to cholesterol-rich membranes (Li and Papadopoulos 1998). A sequence resembling the CRAC motif of cav-1 is present in cav-2, I79-S-K-Y-V-M-Y-K86 (Fig. 1); however, V is replaced by I and the two central aromatic residues of the cav-1 sequence (WF) are replaced by two aliphatic residues in cav-2 (VM). These amino acid sequences directly precede the hydrophobic domains of caveolins.

In 2002, Woodman et al. showed that a sequence shorter than that of the cav-1 CRAC motif comprising only six residues, K96-Y-W-F-Y-R101, was able to bind to membranes, as shown by GFP-fusion experiments (Woodman et al. 2002). However, this motif neither targeted the protein to the cholesterol-rich domain characteristic of caveolae (Woodman et al. 2002) nor promoted the formation of such domains in liposomes (Epand et al. 2003). We recently showed, by CD and NMR measurements, that a peptide comprising the N-MAD (D82-R101) of cav-1 plus the Leu102-Ile109 hydrophobic stretch adopted a helical conformation that was particularly stable towards its C-terminal end in the presence of dodecylphosphocholine (DPC) micelles (Le Lan et al. 2006). A limited number (six) of the residues of this peptide detected the presence of small amounts of phosphatidylserine (POPS) solubilized in DPC micelles, through chemical shift variations, in agreement with the study of Arbuzova et al. (2000). Five of these residues belong to the CRAC motif: V94 and the doublets K96-Y97 and Y100-R101.

```
Cav-1(94-102)  VTKYWFYRL

Cav-2(79-87)   ISKYVMYKF

Cav-3(67-75)   VSKYWCYRL
```

Fig. 1 Amino acid sequence of the cav-1 and cav-2 studied peptides and the homologous sequence in cav-3

Considering the role of this atypical membrane attachment sequence and the incomplete structural information gained from it in our previous work on the cav-1 (D82-I109) peptide, we decided to focus on small peptides encompassing this amino acid sequence, adopting the same strategy as Epand et al. (2005).

The first amino acid of the hydrophobic amino acid stretch downstream from the cav-1 CRAC motif is a highly conserved hydrophobic residue (L102). In line with our strategy based on favoring peptide attachment to membranes (Le Lan et al. 2006), we included hydrophobic residues at the C-terminus of the designed cav-1 and cav-2 peptides: V94-T-K-Y-W-F-Y-R-L102 and I79-S-K-Y-V-M-Y-K-F87, respectively.

We report here the structure and dynamic properties of the cav-1(94–102) peptide in aqueous solution and in interaction with various membrane models. To obtain this information at the atomic level, we chose DPC micelles as membrane mimics because they were already shown to be adequate for such studies, including NMR, primarily due to their small sizes and to the detergent head group being similar to that of phosphatidylcholine (Beswick et al. 1999; Lauterwein et al. 1979; Zhang et al. 2008; see also, e.g., Nanga et al. 2008; Neumoin et al. 2007; Schibli et al. 2006 for recent studies). We also chose DM, a widely used detergent in membrane protein studies, as it often preserves their activities well (Lund et al. 1989; Rosevear et al. 1980) and allows some membrane protein crystallization (Bocquet et al. 2009; Roche et al. 2006). DM was also shown, in CD and fluorescence studies, to be appropriate for peptide folding (Coïc et al. 2005; Sjögren et al. 2005; Vincent et al. 2007; Wimmer et al. 2006).

The interaction of the peptide with these detergents and phospholipid-detergent (DM) micelles was investigated by steady-state fluorescence and circular dichroism studies. The location of the single Trp residue W98 in DM and DPC micelles was assessed by fluorescence quenching with brominated DM analogs and acrylamide. We studied peptide dynamics in buffer, DM, and DPC micelles, by W98 time-resolved fluorescence. The structure of cav-1(94–102) in DPC micelles was determined by NMR. The structural characteristics of cav-2(79–87) and cav-1(94–101) in DPC micelles were also studied for comparison.

Materials and methods

Solutions and chemicals

n-Dodecyl-*β*-D-maltoside (DM) was obtained from Calbiochem. Its brominated derivatives, 7,8-dibromododecylmaltoside (BrDM) and 10,11-dibromoundecanoylmaltoside (BrUM), were synthesized as previously described (de Foresta et al. 1996, 1999). DPC and DPC-d_{38} were purchased from Anatrace and Cortecnet, respectively. *N*-acetyltryptophanamide (NATA), acrylamide, and azide were purchased from Sigma–Aldrich. 1,2-Dimyristoyl-sn-glycero-3-phospho-L-serine (DMPS; sodium salt), 1,2-dimyristoyl-sn-glycero-3-phosphate (DMPA; monosodium salt), 1,2-dimyristoyl-sn-glycero-3-phosphocholine (DMPC), and 1,2-dimyristoyl-sn-glycero-3-[phospho-rac-(1-glycerol)] (DMPG; sodium salt) were obtained from Avanti Polar lipids (AL, USA).

Preparation of DM/phospholipid mixed micelles

The mixed micelles were prepared at a 9:1 (DM: phospholipid) molar ratio in buffer with 180 mM DM and 20 mM DMPS, DMPG, DMPC, or DMPA. Powdered phospholipids were added to the DM solution, and the mixture was vortexed for 2 min and sonicated in a sonication bath at 30°C for 3 min.

Peptide synthesis

The cav-1 peptides (94–102 and 94–101) and the cav-2(79–87) peptide were synthesized by Ansynth Service (LE Roosendaal, NL). They were acetylated at their N-termini and amidated at their C-termini. All peptides were delivered at a purity >95% (HPLC, MALDI/TOF). For fluorescence and CD experiments, a stock solution of cav-1(94–102) was prepared in water at a concentration of 1 mM with 0.016% azide.

Circular dichroism

Far UV circular dichroism spectra were recorded on a Jobin–Yvon CD6 spectropolarimeter calibrated with *d*-10-camphorsulfonic acid. Measurements were performed at room temperature, using 0.5 mm path length quartz cuvettes (Hellma) for 100 μM cav-1(94–102) peptide solubilized in 10 mM sodium phosphate buffer, pH 7.5, alone or in the presence of either 4 mM DPC or DM or DM/lipid (9:1). Spectra were recorded at room temperature in the 185 to 260 nm wavelength range, at 0.5 nm resolution steps, an integration time of 2 s, and a bandwidth of 2 nm. Spectra were averaged over four scans and corrected for background. Concentration was determined by measuring UV absorbance at 280 nm, using an extinction coefficient at 280 nm of 8,250 M^{-1} cm^{-1}, calculated from the amino acid composition of the peptide (Pace et al. 1995).

Steady-state fluorescence measurements

Fluorescence emission spectra for the cav-1(94–102) peptide (5 μM) solubilized in 10 mM sodium phosphate

buffer, pH 7.5, alone or in the presence of either 4 mM DPC or DM or 6 mM DM/phospholipid (9:1) were recorded in a thermostatically controlled cell-holder on a Spex Fluorolog spectrofluorimeter. For reference, a similar experiment was carried out with NATA in 10 mM sodium phosphate buffer, pH 7.5. λ_{ex} was set at 280 nm. Slit widths were 1.25 mm (bandwidths ~5 nm). Spectra were recorded after a short period of equilibration (2–3 min). Emission spectra were normalized. For experiments in which fluorescence was quenched with acrylamide, a stock solution of 5 M acrylamide in water was prepared. Buffers were filtered through Millex-HA filters (0.45 μM pore size; Millipore).

Partitioning of cav-1(V94-L102) between buffer and various pure or mixed detergent micelles

We studied the partitioning of cav-1(94–102) in various micelles by monitoring the changes in fluorescence intensity of the peptide with increasing detergent concentration, at a fixed emission wavelength (332 nm) on the Spex instrument, essentially as previously described (Coïc et al. 2005). Briefly, we sequentially added aliquots of DM, DPC, or mixed DM/phospholipid stock solutions to a 5 μM cav-1(94–102) solution in 10 mM sodium phosphate buffer, pH 7.5, in the fluorescence cuvette at 20°C at 100-s intervals with continuous stirring. Fluorescence was continually recorded, as stated in the figure legends. The fluorescence intensities obtained at each detergent concentration were corrected for background (detergent or DM/phospholipid in buffer) and plotted as a function of total detergent concentration.

The interaction of cav-1(94–102) with pure detergent or mixed phospholipid-detergent micelles was analyzed with a partitioning model making no assumption about the mechanism underlying the interaction. A molar partition coefficient, K (Ben-Tal et al. 1996; Murray et al. 1998; Peitzsch and McLaughlin 1993; Santos et al. 2003; Seelig 2004; Tamm 1991), can be defined (for an excess of detergent over peptide) as the ratio between the molar concentrations of the peptide within the micellar phase and in the bulk aqueous phase:

$$K = \left([P]_m/[D]_m\right)/\left([P]_{H_2O}/[H_2O]\right) \quad (1)$$

where $[P]_m$ and $[P]_{H2O}$ are the peptide concentrations in each phase and $[D]_m$ and $[H_2O]$ are the concentrations of detergent in the micellar phase and water molarity, respectively. When $[P]_m = [P]_{H2O}$, then $K = [H_2O]/[D]_{m1/2}$, where $[D]_{m1/2}$ is the detergent concentration in micelles for half-partitioning.

It can be shown that the ratio of bound to total peptide concentrations is related to K by:

$$[P]_m/[P]_t = K[D]_m/\left([H_2O] + K[D]_m\right) \quad (2)$$

where $[P]_t$ is the total peptide concentration.

If bound and free peptides have different quantum yields, then $[P]_m/[P]_t$ is related to the fluorescence intensity by:

$$[P]_m/[P]_t = (I - I_0)/(I_{max} - I_0) \quad (3)$$

where I_0 and I_{max} are the fluorescence intensities in the absence and presence, respectively, of a detergent concentration resulting in complete peptide binding. Combining Eqs. 2 and 3 gives

$$I = I_0 + (I_{max} - I_0)K[D]_m/([H_2O]+K[D]_m) \quad (4)$$

with $[D]_m = [D]_t - cmc$, where $[D]_t$ is the total detergent concentration and cmc is the critical micellar concentration.

Data points are the means of duplicate measurements for DM and DM/phospholipid (with DMPC and DMPS as a lipid). K was determined by fitting the binding curve, using Eq. 4, for detergent concentration above the cmc. The partitioning free energy, ΔG, was calculated using the formula $\Delta G = -RT\ln K$.

Spectral decomposition of steady-state fluorescence emission spectra

The steady-state fluorescence spectra were analyzed with two-four-parameter log-normal functions (a skewed Gaussian equation) of the following form (Burstein et al. 2001; Burstein and Emelyanenko 1996):

$$I(v) = I_m \exp\left\{-\left(\ln 2/\ln^2 \rho\right) \times \ln^2[(a - v)/(a - v_m)]\right\} \quad (\text{at } v < a)$$

$$I(v) = 0 \quad (\text{at } v \geq a)$$

Here, $I_m = I(v_m)$ is the maximum fluorescence intensity, v_m is the wavenumber of the band maximum (peak), $\rho = (v_m - v_-)/(v_+ - v_m)$ is the band asymmetry parameter, v_+ and v_- are the wavenumber positions of left and right half-maximum amplitudes, a is the function-limiting point: $a = v_m + \text{FWHM}\ \rho/(\rho^2 - 1)$, and the full width at half-maximum (FWHM) $= v_+ - v_-$.

We fitted a linear combination of this analytical model to the emission spectra by the least squares regression method (KaleidaGraph, Synergy Software, PA, USA).

Analysis of the data for fluorescence quenching with acrylamide and brominated detergents

Fluorescence was quenched with acrylamide, essentially as previously described (Tortech et al. 2001). Peptide

quenching in detergent micelles was analyzed with the classical Stern-Volmer equation (for reviews, see Eftink 1991; Lakowicz 1999):

$$F_0/F = 1 + K_{sv}[Q]$$

where F_0 and F are the fluorescence intensities in the absence and presence of quencher, respectively, K_{sv} is the Stern–Volmer quenching constant, and $[Q]$ is the quencher concentration. K_{sv} is related to the bimolecular quenching constant k_q by the following formula:

$$K_{sv} = k_q \tau_0$$

where τ_0 is the lifetime, in the absence of quencher, of the fluorophore.

In our case, where the intensity decays are multiexponentials, τ_0 was replaced by the intensity average lifetime $<\tau>_f$ calculated as $<\tau>_f = \sum \alpha_i \tau_i^2 / \sum \alpha_i \tau_i$, according to Sillen and Engelborghs (1998).

For NATA, taken as a reference, and peptide in buffer we used the nonlinear Stern-Volmer equation:

$$F_0/F = (1 + K_{sv}[Q])\exp V[Q]$$

where V can be considered as a sphere of action around the fluorophore in which the presence of a quencher molecule results in instantaneous (static) quenching.

Fluorescence quenching experiments were carried out with cav-1(94–102) solubilized in mixed micelles of DM with a brominated analog (BrDM or BrUM), essentially as previously described (de Foresta et al. 2002). Data were analyzed with a lattice model of quenching (East and Lee 1982; London and Feigenson 1981; Powl et al. 2005). This model was originally designed to describe the quenching of membrane fluorophores (e.g., protein Trp) by spin-labeled or brominated phospholipids. It considers two populations of fluorophores: one completely inaccessible to the quencher and responsible for the residual fluorescence F_{min} (e.g., Trp embedded in a protein), whereas in the other population, each fluorophore has n neighbors (phospholipids) and fluorescence is completely quenched if one (or more) of these sites is occupied by a modified phospholipid (corresponding to a quenching efficiency of 100% upon contact). It is assumed that phospholipids do not change position during the lifetime of the fluorophore. If X is the molar fraction of quenchers in the membrane, then $(1 - X)^n$ is the probability that none of the n sites is occupied by a quencher. The fluorescence ratio is therefore given by: $F/F_0 = (1 - F_{min}/F_0)(1 - X)^n + F_{min}/F_0$.

In a micellar environment, unlike in lipid bilayers, the "lattice parameter" n is not expected to give an exact determination of quenchers around Trp because some dynamic quenching may occur in addition to static quenching (de Foresta et al. 1999, 2002) and because the transverse inaccessibility of Trp is not taken into account directly in the model. The parameter n is, however, correlated with the accessibility of this residue to brominated alkyl chains. We previously described variations of n with Trp depth from quenching curves, with BrDM and BrUM, for a set of six model peptides (P_n) with Trp at various positions in the sequence (positions 3, 5, 7, 9, and 13 in the 25-amino acid sequence; de Foresta et al. 2002). These data were used as the reference in this study.

Time-resolved fluorescence measurements

Fluorescence intensity and anisotropy decays were obtained by the time-correlated single-photon counting technique from the polarized $I_{vv}(t)$ and $I_{vh}(t)$ components. Most experiments were performed as previously described (Vincent et al. 2005), except that a light-emitting diode (PLS 295, from Picoquant, Berlin-Adlershof, Germany; maximum emission at 298 nm) was used as an excitation source and a Hamamatsu photomultiplier (model R3235-01) was used for detection. As previously described, fluorescence intensity $I(t)$ and anisotropy decays $r(t)$ were analyzed as sums of 150 or 100 exponential terms, respectively, by the maximum entropy method (MEM; Livesey and Brochon 1987), using multiexponential models: $I(t) = \sum \alpha_i \exp(-t/\tau_i)$, where α_i is the normalized amplitude of the lifetime τ_i, and $r(t) = \sum \beta_i \exp(-t/\theta_i)$, where β_i is the contribution to the anisotropy of the rotational correlation time θ_i. In this second analysis, we assumed that each lifetime τ_i is associated with all rotational correlation times θ_i. MEM does not impose any particular number of significant parameters for the decay. The Skilling-Jaynes entropy S was subjected to a χ^2 constraint (Brochon 1994) to ensure that the recovered distribution was consistent with the data.

According to Perrin (Perrin 1936), the Brownian rotational correlation time (θ) is proportional to the hydrated volume of the particle (V_h) and to the viscosity/temperature factor (η/T) such that $\theta = V_h \eta / RT$.

NMR experiments

Peptides were dissolved at a concentration of 3.5 mM in 90/10 (v/v) H_2O/D_2O, containing 100 mM perdeuterated DPC-d_{38} for cav-1(94–102) and for cav-2(79–87). The DPC concentration used corresponds to that needed to obtain a plateau in titration curves of proton chemical shifts as a function of DPC concentration (data not shown). DPC titrations were performed by adding small aliquots of an 800 mM DPC stock solution to a 3.5 mM peptide solution (90/10 H_2O/D_2O). For cav-1(94–101), a higher DPC

concentration (400 mM) was required. The pH was adjusted to 5.5 in all experiments.

Spectra were recorded at 20 and 30°C on a DRX Brucker spectrometer operating at 600 MHz or at 500 MHz ^{1}H frequency, equipped with a cryoprobe and an X-^{1}H inverse probehead, respectively. Chemical shifts were expressed with reference to internal standard dimethylsilapentane-sulfonic acid, sodium salt (DSS). Standard two-dimensional total correlated spectroscopy (TOCSY) and nuclear Overhauser effect spectroscopy (NOESY) spectra were recorded with mixing times of 70 ms (TOCSY) and 150 and 300 ms (NOESY). Signals were assigned with the standard protocol (Wüthrich 1986). For the ^{13}C chemical shift assignments, natural abundance ^{1}H-^{13}C HSQC (heteronuclear single quantum correlation) spectra were recorded.

We localized the cav-1(94–102 and 94–101) and cav-2(79–87) peptides in DPC micelles on the basis of intermolecular NOEs with the DPC signals. For this, we compared NOESY spectra (500 ms mixing time) of peptide solutions in perdeuterated DPC-d_{38} micelles with or without protonated DPC (10%) in D_2O.

The accessibility to solvent of the amide backbone protons was determined by proton/deuterium exchange studies. We prepared samples by solubilizing 3.5 mM cav-1(94–101) and cav-1(94–102) in 400 mM and 100 mM DPC-d_{38}, respectively, in H_2O, pH 5.5, and further freeze-drying the mixture. Series of 1D NMR spectra were recorded just after solubilization of the peptide/DPC samples in D_2O. Solvent accessibility was monitored by following the disappearance of the amide proton signal.

Molecular modeling of cav-1(94–102)

The structure of cav-1(94–102) in the presence of 100 mM DPC-d_{38} was determined from NOESY spectra recorded at 20°C with a mixing time of 100 ms. Sybyl version 7.1 (Tripos, St. Louis, MO, USA) was used for modeling. The Tripos force field with electrostatics was used for minimization and dynamics. Interresidue distance ranges derived from NOE data were entered as constraints. Based on NOE intensities, the upper limit of proton-proton distance ranges was set to 3, 4, or 5 Å and the lower limit to 1.8 Å. No hydrogen bond was imposed. The molecule was then subjected to simulated annealing from 800 to 0 K for 5 ps. One hundred cycles were run. Ten structures with significantly lower energy than the others were selected. They were then minimized by alternating short low-temperature dynamics (2 ps, 20 K) and minimization runs until the potential energy remained stable.

Results

Cav-1(94–102) interaction with pure detergent or lipid-detergent micelles: titration by steady-state fluorescence intensity measurements

The interaction of cav-1(94–102) with DM and DPC micelles results in significant Trp (i.e., W98) fluorescence changes, such as a blue-shift of the fluorescence emission spectrum, together with an increase in fluorescence intensity. Interaction with the micelles was studied by monitoring the increase in fluorescence intensity, at a fixed emission wavelength, as a function of total detergent concentration (Fig. 2a). For DPC, the titration curve had a sigmoid shape, with fluorescence intensity starting to increase at $\sim$0.5 mM DPC and reaching a plateau at detergent concentrations greater than 2 mM. The midpoint of the curve was close to the cmc value of pure DPC ($\sim$1.1 mM; Brown et al. 1981; Lauterwein et al. 1979), indicating that peptide–detergent interaction occurred even below the concentration required for pure detergent micelle formation. By contrast, the titration curve obtained with DM (Fig. 2a) displayed a continuous slight increase in fluorescence intensity, which reached only half the value corresponding to the plateau obtained with DPC at the highest DM concentration used (6 mM), which was well above the cmc of DM ($\sim$0.18 mM; le Maire et al. 2000). This absence of plateau in the presence of DM, as compared to DPC indicates that cav-1(94–102) interacts more strongly with DPC than with DM micelles. If we assume a simple model of cav-1(94–102) partitioning into detergent micelles (without specific interaction), the titration curve obtained with DM as the detergent corresponds to an estimated molar partition coefficient K of 5.5×10^3, a value at least one order of magnitude lower than that estimated with DPC ($K > 50 \times 10^3$ taking $K > [H_2O]/[D]_{m1/2} \sim 55$/cmc, see "Materials and methods").

We carried out additional cav-1(94–102) partitioning experiments with various DM/phospholipid mixed micelles to investigate further the possible role of specific interactions of the peptide with polar head groups that might account for the differences in behavior of these two detergents and contribute to peptide interaction with biological membranes. These micelles contained small amounts of either zwitterionic or anionic phospholipids (DM/phospholipid = 9:1, mol/mol), bearing an acyl chain similar in length to that of the detergents. As shown in Fig. 2b DMPC, a zwitterionic lipid with the same polar head group as DPC, had no significant effect on the titration curve of the cav-1 peptide with mixed micelles, whereas the anionic lipid DMPS strongly favored partitioning, which was already complete at concentrations

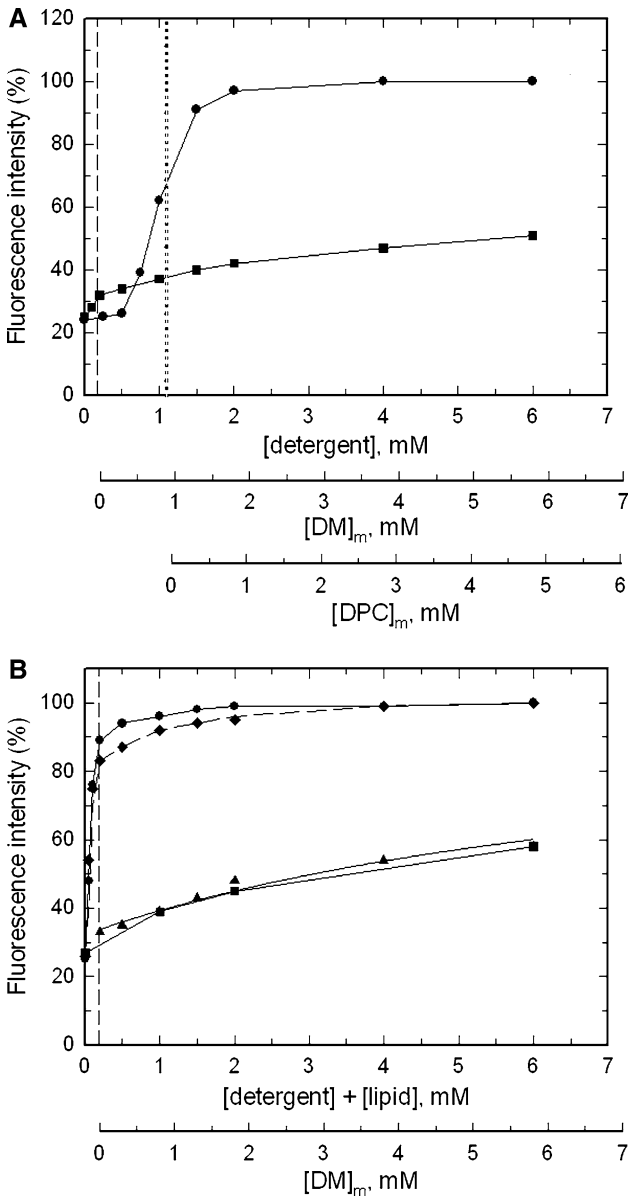

Fig. 2 Binding of cav-1(94–102) to various pure detergent micelles (**a**) or mixed micelles of DM/lipid (**b**). **a** We added 5 μM cav-1(94–102) to 10 mM sodium phosphate buffer, pH 7.5, at 20°C. Aliquots of DM (*squares*) or DPC (*circles*) were then added sequentially. Fluorescence was recorded continuously with λ_{ex} and λ_{em} set at 280 and 332 nm, respectively (slit width = 1.25 mm for both excitation and emission). Detergent cmcs are indicated as a *dotted line* for DPC and a *dashed line* for DM. A curve was fitted to the data as described in "Materials and methods". Theoretical scales of micellar detergent $[D]_m$ (see "Materials and methods") for DM and DPC are represented below the *[Detergent]* scale. **b** The experiment was performed as for **a** with mixed micelles of DM/lipid (9:1, mol/mol), including DM/DMPC (*triangle*), DM/DMPS (*dashed line*), DM/DMPG (*diamond*), or DM/DMPA (*circle*), which were compared with DM alone (*square*). The cmc for DM is indicated as a *dashed line*. Curves were fitted to the DM and DM/DMPC data as described in "Materials and methods." As in **a**, a theoretical scale of $[D]_m$ is shown

close to the cmc of DM. Thus, based on an analysis similar to that described above, we can estimate that K was greater than 275×10^3. DMPA and DMPG were equally efficient at increasing the partitioning of the peptide in DM micelles. In addition, increases in ionic strength (with 150 mM NaCl) decreased the partitioning of the peptide in mixed DM/DMPS micelles (data not shown). Interpretation of these results in terms of DPC and DM micelle properties and of nonspecific electrostatic interactions is further discussed below.

Change in the polarity of the microenvironment of W98 upon the interaction of cav-1(94–102) with pure detergent or lipid-detergent micelles: steady-state fluorescence emission spectra

In buffer, the maximum emission wavelength λ_{max} of cav-1(94–102) was 348 nm, close to that of NATA (λ_{max} = 353 nm) and indicative of a highly polar environment for Trp (Fig. 3a). By contrast, in the presence of 4 mM detergent (DM or DPC), we observed a strong blue shift of the spectra, with λ_{max} = 332 and 333 nm in DPC and DM, respectively, indicative of a more hydrophobic Trp environment. Consistent with this change in polarity, these blue shifts were correlated with increases in maximum fluorescence intensity by factors of 3.5 and 1.7 in DPC and DM, respectively. The decomposition of these emission spectra into log-normal Gaussians yielded only one spectral component for the peptides in buffer. By contrast, in both detergents, the same procedure yielded two spectral components with maxima at 324–326 and 342–344 nm (Table 1). These two elementary spectra characterize two environments with very different polarities. The data for DPC micelles, in which peptide partitioning was more favorable, suggest that the W98 residue was present at two locations within micelles: one more exposed to the aqueous solvent, at the water/micelle interface, and the other more deeply embedded in the micelle. The higher proportion of the more "polar" spectrum in DM micelles than in DPC micelles is consistent with the incomplete partitioning of the peptide into micelles in these conditions, as described above.

Figure 3b shows a comparison of the fluorescence spectrum for cav-1(94–102) in DM-DMPS mixed micelles and DM micelles. The presence of DMPS resulted in a 6 nm blue-shift of the emission spectrum (from λ_{max} = 333 nm in DM micelles to λ_{max} = 327 nm in DM/DMPS mixed micelles) together with a 1.7-fold increase in maximum fluorescence intensity, consistent with a considerable

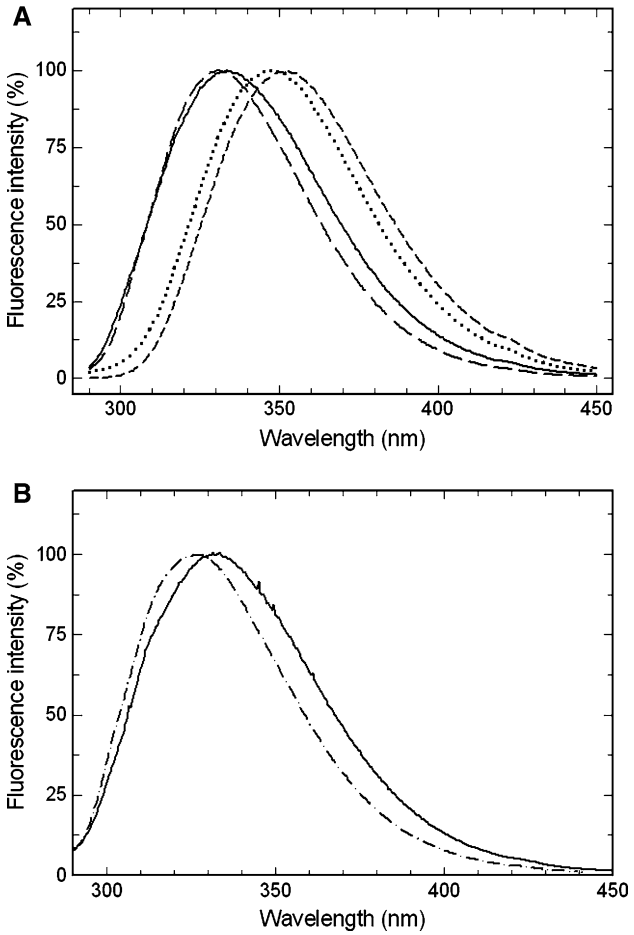

Fig. 3 Fluorescence emission spectra for the cav-1(94–102) peptide in various pure micelles (**a**) or mixed micelles of DM/lipid (**b**). **a** Normalized emission spectra for cav-1(94–102) peptide (5 μM) in 10 mM sodium phosphate buffer, pH 7.5, alone (*dotted line*) and supplemented with 4 mM DPC (*medium dashed line*) and DM (*solid line*), at 20°C. For reference, a similar experiment was performed with NATA in 10 mM sodium phosphate buffer, pH 7.5 (*line of short dashes*). λ_{ex} was set at 280 nm (slit width = 1.25 mm for both excitation and emission). **b** The experiments were performed as for **a**, with mixed micelles of DM/DMPS (9:1, mol/mol, 6 mM total concentration; *dashed dotted line*) and DM micelles (*solid line*)

strengthening of peptide binding in the presence of DMPS, as described above. Decomposition of the experimental fluorescence emission spectrum yielded two elementary spectra, both significantly blue-shifted with respect to that of pure DM micelles (Table 1).

Cav-1(94–102) conformation in pure detergent and in mixed micelles: CD study

We investigated the secondary structure of the cav-1(94–102) peptide by carrying out a far-UV CD study of this peptide in phosphate buffer in the presence and absence of DPC and DM micelles (Fig. 4a). The aromatic side chains of four of the nine amino acids of the sequence contribute to the far UV CD of the peptide, but it was nonetheless possible to do a qualitative evaluation of the presence of secondary structures (Krittanai and Johnson 1997; Rogers and Hirst 2004). The spectrum of the cav-1 peptide solubilized in buffer displayed a broad negative peak at about 195 nm, consistent with a predominantly random coil-like conformation. The CD spectrum of the cav-1 peptide was radically altered in the presence of DPC micelles, indicating the occurrence of structural changes following interaction with zwitterionic micelles. The negative CD ellipticity around 195 nm observed for the peptide in buffer disappeared with the concomitant increase in a CD band centered at ~191 nm and the appearance of two negative bands centered at ~208 and ~222 nm. This CD spectrum is characteristic of a predominantly helical conformation. In the presence of DM micelles, the negative ellipticity observed at ~191 nm in buffer was smaller and the negative ellipticity at 222 nm was greater. These spectral characteristics suggested that the proportion of the peptides in the α-helical state was larger in DM than in buffer. However, the percentage of peptides in the α-helical state was lower in DM than in DPC. The structural changes induced by these detergents are consistent with the

Table 1 Parameters of the log-normal Gaussian components of the steady-state fluorescence emission spectra of cav-1(94–102) in various detergent micelles and buffer

Sample	Raw spectrum λ_{max} (nm)	Log-normal Gaussian #1			Log-normal Gaussian #2		
		λ_{max} (nm)	FWHM (cm^{-1})	Spectrum peak height (%)	λ_{max} (nm)	FWHM (cm^{-1})	Spectrum peak height (%)
NATA							
Phosphate buffer	352.5	352.5	4,826	100	_	_	_
Cav-1(94–102)							
Phosphate buffer	347	347	4,869	98	_	_	_
DPC micelles	332	342	4,610	33	326	4,459	67
DM micelles	333	344	4,780	43	324	4,827	57
DM/DMPS							
Mixed micelles	327	332	4,996	52	319	4,428	48

The spectra are presented in Fig. 3. The steady-state fluorescence spectra were analyzed as described in "Materials and methods"

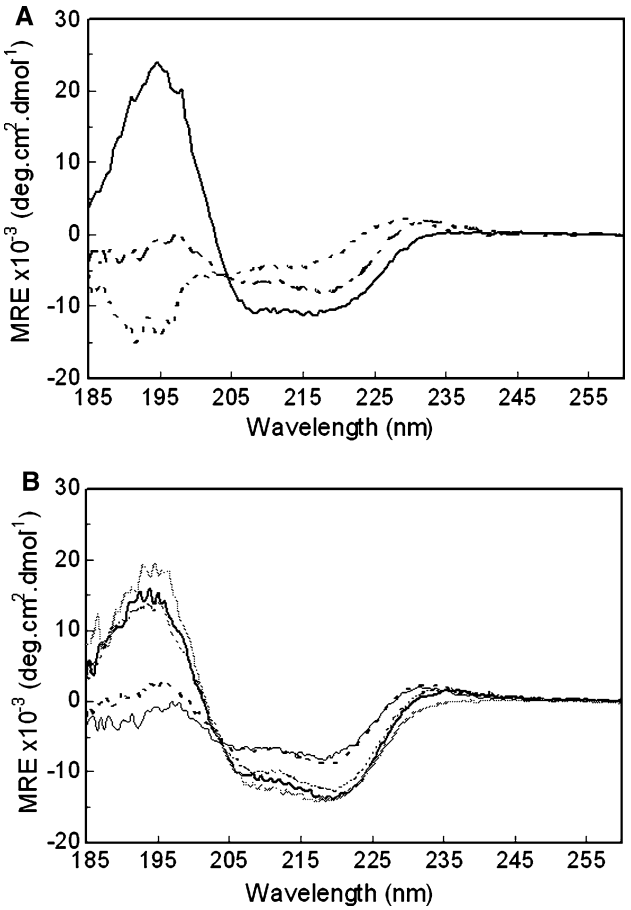

Fig. 4 Far UV CD spectra of cav-1(94–102) peptide in various pure detergent micelles (**a**) and mixed micelles of DM/lipid (**b**). **a** Spectra were registered with 100 μM cav-1(94–102) in 10 mM sodium phosphate buffer, pH 7.5, (*dashed line*) and in the presence of 4 mM DPC (*continuous line*) and DM (*dashed dotted line*). Further details are provided in "Materials and methods." **b** Spectra were registered as for **a**, with mixed micelles of DM/lipid (9:1, mol/mol), DMPA (*short dotted line*), DMPG (*solid thick line*), DMPS (*dotted line*), and DMPC (*dashed line*) as the lipid. The CD spectrum in DM (*solid thin line*) was added for comparison

differences in peptide partitioning into DM and DPC micelles inferred from W98 fluorescence measurements.

In the presence of anionic lipids, we observed an increase in the band of positive CD centered at ~191 nm and a decrease in the two negative bands centered at ~208 and ~222 nm with respect to what was observed with DM alone (Fig. 4b). These results suggest that a larger proportion of the peptides were in an α-helical state in these conditions. Moreover, zwitterionic lipid DMPC had no significant structuring effect.

These CD results, together with the fluorescence data, indicate that peptide partitioning into the various mixed lipid-detergent micelles is coupled with changes in peptide structure.

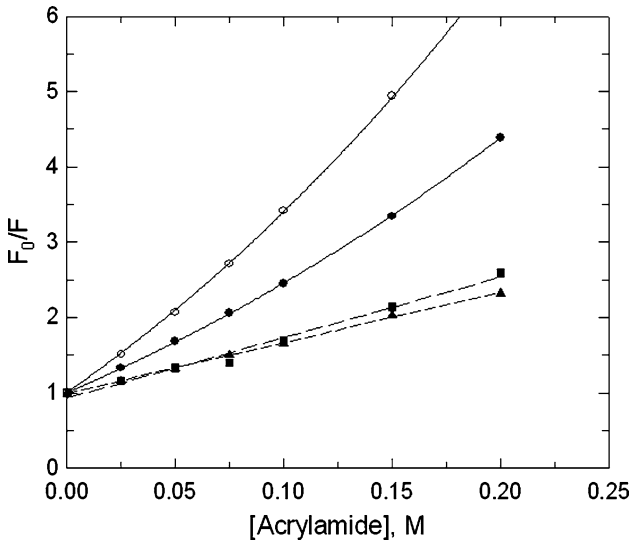

Fig. 5 Stern-Volmer plots of the quenching by acrylamide of cav-1(94–102) peptide fluorescence in various media. The experiments were performed with cav-1(94–102; 5 μM) in 10 mM sodium phosphate buffer, pH 7.5, at 20°C in the absence (*closed circles*) or presence of 4 mM DPC (*closed squares*) or DM (*closed triangles*). Aliquots of acrylamide were added sequentially, and Trp fluorescence intensity was recorded with λ_{ex} set at 295 nm (slit width 1.25 mm) and λ_{em} at 340 nm (slit width 2.5 mm). For reference, a similar experiment (but with λ_{em} set at 353 nm) was performed with NATA (5 μM) in water (*open circles*). Data analysis was performed as described in "Materials and methods"

Location of the W98 residue of cav-1(94–102) in DM and DPC micelles: fluorescence quenching by acrylamide and brominated detergents

We evaluated the depth at which the single Trp residue was located within the micelles by carrying out quenching experiments with both acrylamide, as a water-soluble quencher, and two brominated analogs of DM, i.e., BrDM and BrUM (brominated at positions 7–8 and 10–11 of the acyl chain, respectively), as lipid-soluble quenchers.

The Stern-Volmer plots of fluorescence quenching by acrylamide obtained for cav-1(94–102) in micelles were linear, yielding the Stern-Volmer quenching constant K_{sv} (Fig. 5). By comparing the calculated bimolecular quenching constant k_q (Table 2; taking into account the lifetime values measured in similar conditions, see below), we showed that W98 in the peptide in buffer was highly accessible to the water-soluble quencher as compared to NATA, but that accessibility to solvent decreased to ~30% in the presence of either DM or DPC micelles.

With brominated detergents as quenchers, the fluorescence intensity of W98 in cav-1(94–102) was determined as a function of the molar ratio of BrDM or BrUM in DM-BrDM or DM-BrUM mixed micelles. The curves were fitted with Lee's lattice model, as previously described

Table 2 Parameters of cav-1(94–102) fluorescence quenching by acrylamide

Fluorophore	Medium	$<\tau>_f$ (ns)	K_{sv} (M^{-1})	k_q ($M^{-1}s^{-1}$) (%)	V (M^{-1})
NATA	Water	3.0	18.5	6.17×10^9 (100%)	1.76
cav-1(94–102)	Phosphate buffer	2.70	10.9	4.03×10^9 (65%)	1.6
	DPC micelles	4.62	8.02	1.74×10^9 (28%)	_
	DM micelles	4.17	6.70	1.61×10^9 (26%)	_

For the peptide, the intensity average lifetimes $<\tau>_f$ were calculated as $<\tau>_f = \frac{\sum \alpha_i \tau_i^2}{\sum \alpha_i \tau_i}$ with α_i and τ_i values from Table 3. $<\tau>$ for NATA was as reported by Rouvière et al. (1997). K_{sv} and V were obtained from Fig. 5, and k_q was calculated as explained in "Materials and methods"

(see "Materials and methods"; East and Lee 1982; London and Feigenson 1981; Powl et al. 2005; Fig. 6). We found that 70% of the peptide fluorescence was quenched in the presence of pure brominated detergent micelles, consistent with incomplete binding of peptide to these micelles (in 4 mM detergent), as observed for DM micelles. The shape of the quenching curve, characteristic of the properties of the bound peptide, yielded lattice parameters n (3.7 and 4.4 in BrDM and BrUM, respectively) in the range of that obtained for α-helical transmembrane model peptides, P_n (de Foresta et al. 2002).

By comparison with the data for these P_n model peptides in DPC and DM (de Foresta et al. 2002; Vincent et al. 2007), the quenching data of cav-1(94–102) by acrylamide in DPC and DM and by brominated DM in mixed DM/brominated DM micelles are consistent with the W98 residue of the bound peptide being located in the head group region of DPC or DM micelles, as also suggested by the fluorescence spectra.

Conformational heterogeneity and dynamics of cav-1(94–102) peptide in buffer, DM, and DPC micelles: time-resolved fluorescence study

Fluorescence intensity decays yield Trp fluorescence lifetime distributions, which are sensitive indicators of ground-state heterogeneity (such as conformer distribution; Moors et al. 2006; Pan and Barkley 2004) and reactions involving the excited state (energy transfers, dipolar relaxation; Vincent and Gallay 1995). In buffer, a classic lifetime distribution was observed for W98 fluorescence, with an even distribution into three lifetime components (~0.6, 1.7, and 3.9 ns; see Table 3 and Supplementary Material

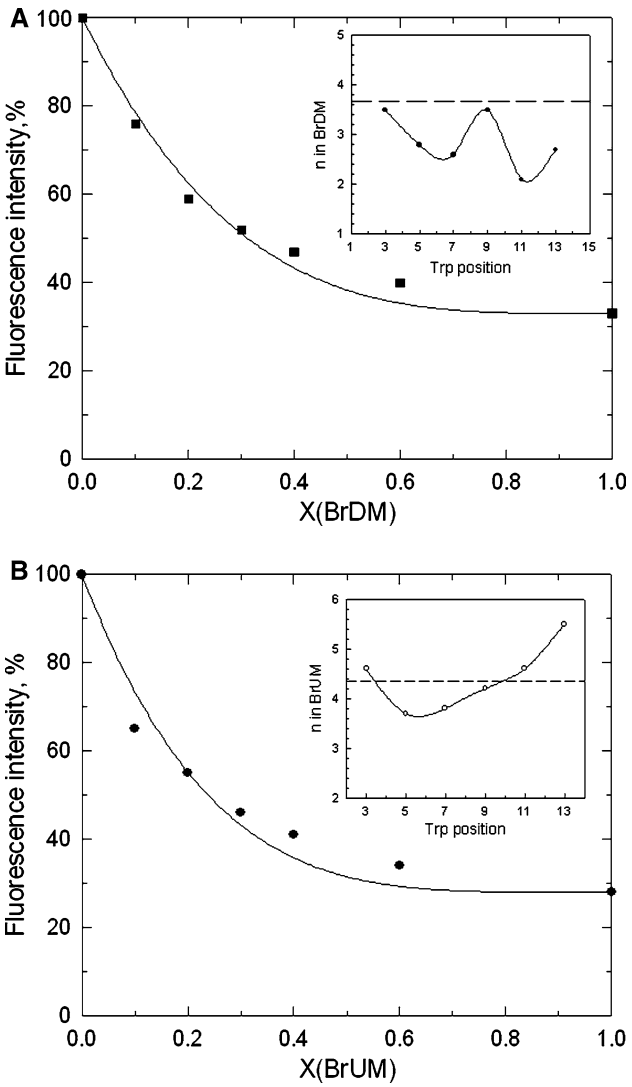

Fig. 6 Quenching of cav-1(94–102) fluorescence in mixed micelles of BrDM/DM (**a**) or BrUM/DM (**b**). Independent measurements of cav-1(94–102; 5 μM) fluorescence intensities were made in 10 mM sodium phosphate buffer, pH 7.5, supplemented with various mixtures of BrDM and DM (**a**), or BrUM and DM (**b**), at a final total detergent concentration of 4 mM at 20°C. The intensities were plotted as a function of X, the molar fraction of the brominated detergent. λ_{ex} was set at 280 nm and λ_{em} at 333 nm (slit width = 1.25 mm for both excitation and emission). A curve was fitted to the data as described in "Materials and methods." The *insets* show the calibration curves of n with Trp position, obtained with six model peptides in BrDM (**a**) and BrUM (**b**) (de Foresta et al. 2002). The *horizontal lines* represent the n values obtained for cav-1(94–102) with BrDM and BrUM

Fig. 1). By contrast, in the presence of DPC micelles, the distribution was characterized by a major long-lifetime component (~5 ns), with two minor shorter lifetimes. This long lifetime component may indicate the presence of one major conformer of the Trp side chain (Bouhss et al. 1996; Willis et al. 1994), consistent with the high α helix content observed on CD. The profile in the presence of DM micelles was more complex, with four lifetime populations,

Table 3 Parameters of the fluorescence intensity decays of cav-1(94–102) peptide in various media

Solvent	α_1	α_2	α_3	α_4	τ_1 (ns)	τ_2 (ns)	τ_3 (ns)	τ_4 (ns)	$<\tau>_a$ (ns)	χ^2
Phosphate buffer	0.28 (±0.05)	0.47 (±0.02)	0.25 (±0.04)	_	0.57 (±0.10)	1.68 (±0.17)	3.88 (±0.18)	_	1.92 (±0.01)	1.07 (±0.02)
DPC micelles	0.20 (±0.03)	0.21 (±0.02)	0.59 (±0.03)	_	0.62 (±0.09)	1.88 (±0.28)	5.13 (±0.09)	_	3.53 (±0.06)	1.06 (±0.02)
DM micelles	0.12 (±0.03)	0.27 (±0.01)	0.33 (±0.02)	0.28 (±0.02)	0.15 (±0.04)	0.85 (±0.09)	2.50 (±0.18)	5.58 (±0.15)	2.63 (±0.07)	1.05 (±0.02)

Cav-1(94–102) peptide was used at concentrations of 150, 50, and 100 μM in buffer, in 40 mM DPC, and in 40 mM DM respectively. $\lambda_{em} = 347$, 330, and 333 nm in buffer, DPC, and DM, respectively, with λ_{ex} centered at 298 nm. The temperature was 20°C. α_i is the normalized area and τ_i the barycenter of each peak of the lifetime distribution obtained in the MEM analysis. The amplitude average lifetime $<\tau>_a$ is calculated as $<\tau>_a = \sum \alpha_i \tau_i$. Data are mean values (±SE) over four experiments

Table 4 Parameters of the fluorescence anisotropy decays of cav-1(94–102) peptide in various media

Solvent	β_1	β_2	θ_1 (ns)	θ_2 (ns)	$r_{t=0}$	χ^2
Phosphate buffer	0.100 (±0.008)	0.142 (±0.001)	0.09 (±0.01)	0.59 (±0.01)	0.247 (±0.002)	1.34 (±0.03)
DPC micelles	0.028 (±0.015)	0.129 (±0.014)	2.27 (±1.43)	10.9 (±0.6)	0.157 (±0.005)	1.11 (±0.05)
DM micelles	0.007 (±0.007)	0.133 (±0.003)	1.1 (±1.1)	14.6 (±1.4)	0.139 (±0.010)	1.10 (±0.01)

Experimental conditions were as described in Table 3. The anisotropy β_i is the area and the rotational correlation time θ_i is the barycenter of peak i of the rotational correlation time distribution. $r_{t=0}$ is the anisotropy at time zero, with $r_{t=0} = \sum \beta_i$. Data are mean values (±SE) over two to three experiments

as in previous experiments (de Foresta et al. 2002). In addition to the various Trp conformations, a heterogeneous environment surrounding Trp in the presence of DM micelles may account for this result (see above). Moreover, the amplitude of the longest lifetime (~30%) is smaller than that in DPC micelles (~60%), again consistent with structural data. As a result, the amplitude average lifetimes $<\tau>_a$ for cav-1(94–102) peptide fluorescence were highest in DPC, lower in DM, and lowest in buffer. As expected, this trend resembles that for steady-state maximum fluorescence intensities (ratio 3.5/1.7/1 with buffer as reference, although measured in slightly different experimental conditions).

Fluorescence anisotropy decays can be used to characterize the rotational dynamics of the systems studied (Table 4). In buffer, we observed a major rotational correlation time in the subnanosecond range ($\theta_2 \sim 0.6$ ns), corresponding to the Brownian motion of the peptide. A shorter correlation time ($\theta_1 = 100$ ps) was also observed, describing the fast local motion of the Trp side-chain around the Cα–Cβ–Cγ bonds. In DM and DPC micelles, both correlation time values were about one order of magnitude higher, reflecting the incorporation of the peptide into detergent micelles. The longer correlation times (11 and 15 ns for DPC and DM, respectively) were in the range expected for these detergent micelles, indicating that peptide-detergent complexes and pure micelles are similar in size.

Structure of the cav-1(94–102) peptide in deuterated DPC micelles, as determined by NMR

CD spectroscopy showed that the cav-1(94–102) peptide was mostly folded as an α-helix in DPC micelles. This folding was characterized in greater detail by ^{1}H and ^{13}C NMR spectroscopy. In H_2O, the H_α index profile of the peptide (data not shown) displayed weak negative values (-0.1 ppm $< \Delta\delta H_\alpha < -0.2$ ppm), typical of an unstructured conformation. The addition of deuterated DPC micelles had a major effect on the peptide spectra, indicating an interaction between DPC molecules and the peptide within mixed micelles, resulting in a change in peptide conformation. Most of the proton and carbon resonances of cav-1(94–102) spectra were assigned. The $^{13}C_\alpha$ chemical shift indices, defined as differences in the $^{13}C_\alpha$ chemical shifts between observed and random coil values, were used to identify the secondary structure (Wishart et al. 1995). $^{13}C_\alpha$ chemical shifts are known to be particularly sensitive to the backbone structure of the polypeptide chain, whereas H_α chemical shifts tend to be more strongly influenced by ring current and sequence effects. The long series of positive $^{13}C_\alpha$ indices ($\Delta\delta C_\alpha > 0.7$ ppm; Fig. 7a) provided evidence for a predominantly helical conformation. Surprisingly, these values were very large (up to 2.2 ppm) for such a small peptide (nine residues), revealing a stable helical conformation. The lower $^{13}C_\alpha$ indices for R101 and L102 indicate some fraying at the C-terminal end

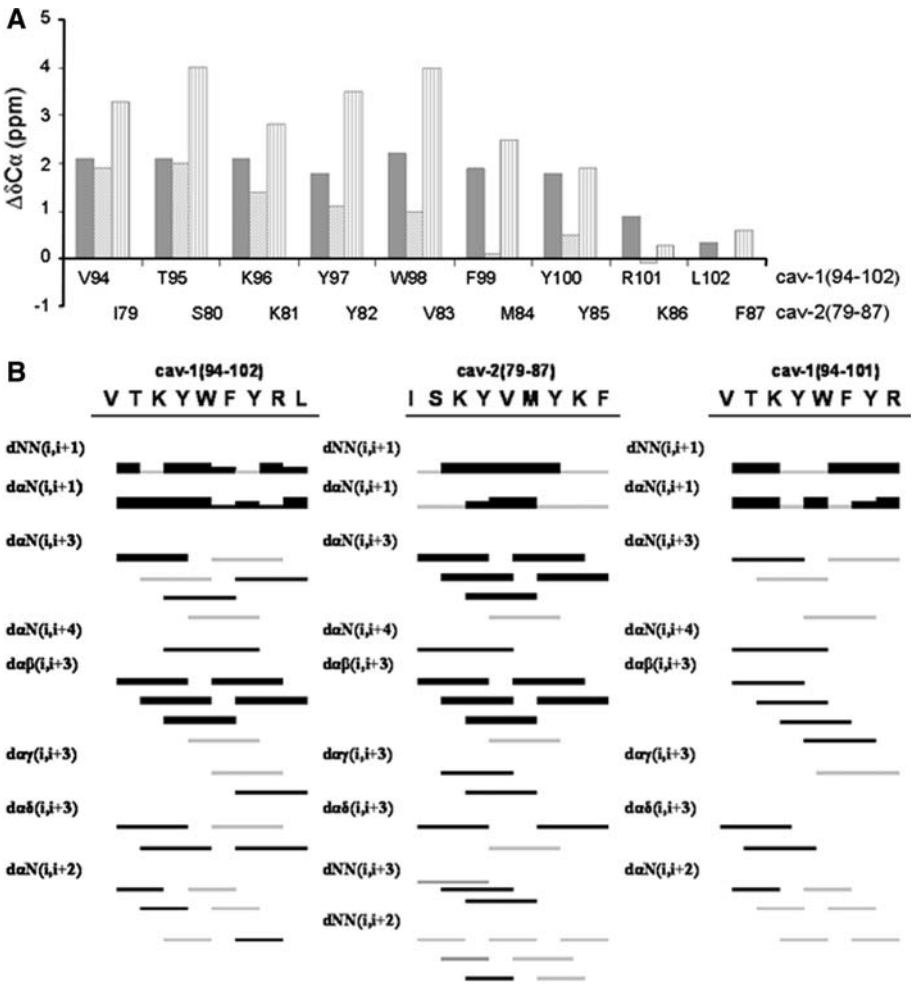

Fig. 7a, b NMR analysis of cav-1 and cav-2 peptides in DPC micelles. **a** $^{13}C_{\alpha}$ chemical shift indices ($\Delta\delta C_{\alpha}$) for cav-1(94–102) (*dark gray bar*), cav-1(94–101) (*gray bar*), and cav-2(79–87) (*striped gray bar*) solubilized in DPC micelles. See "Materials and methods" for details. **b** Sequential and medium NOE connectivities for the cav-1(94–102), cav-2(79–87), and cav-1(94–101) peptides solubilized in DPC micelles at 293 K, from a 2D NOESY spectrum (100 ms mixing time). The thickness of the *black bar* indicates NOE intensity (strong, medium, weak). *Gray bars* indicate ambiguous NOEs

of the helix. The presence of intense sequential dNN(i, i + 1) NOEs and (i, i + 3)/(i, i + 4) correlations provides further evidence of the existence of a helical conformation along the entire length of the peptide (Fig. 7b, left panel). We then carried out molecular modeling of cav-1(94–102), using NOEs as distance constraints. As expected from the characteristic NOE network, the structures obtained from simulated annealing and minimization cycles had a helical conformation from V94 to L102 (Fig. 8). The average positions of specific side chains in peptide modeling were of particular interest. The two tyrosine residues (97 and 100) were on the same face of the helix and were surrounded by the two charged residues, Arg101 and Lys96, whereas the aromatic residues Trp98 and Phe99 were located on the opposite face of the helix. This side-chain positioning is typical of an amphipathic helix.

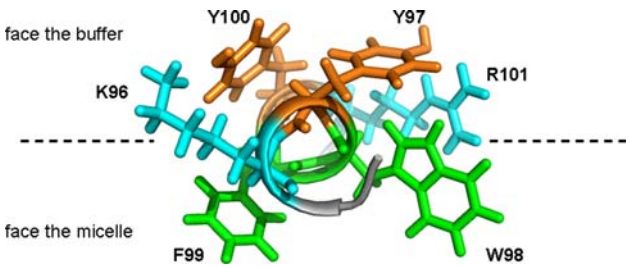

Fig. 8 NMR model of cav-1(94–102) peptide**.** The structure of cav-1(94–102) in the presence of 100 mM DPC-d38 was determined from NOESY spectra (100 ms mixing time, 20°C). The *dashed line* allows visualization of the most probable orientation of the helix. The most recent version of Sybyl (version 7.1; Tripos, St. Louis, MO) was used for modeling. The Tripos force field with electrostatics was used for minimization and dynamics. Further details are provided in "Materials and methods"

NMR comparison of the structural properties of the cav-2(79–87) and cav-1(94–102) peptides in DPC micelles

The C-terminal sequences of the N-terminal attachment domains of cav-2 and cav-1 (residues 79–87 and 94–102, respectively) differed, as shown in Fig. 1. In particular, the two central aromatic residues (W–F) of the cav-1 sequence were replaced by two aliphatic residues (VM) in cav-2. We compared the structural properties of these two amino acid sequences by carrying out an NMR study of the cav-2(79–87) peptide under the same experimental conditions as used

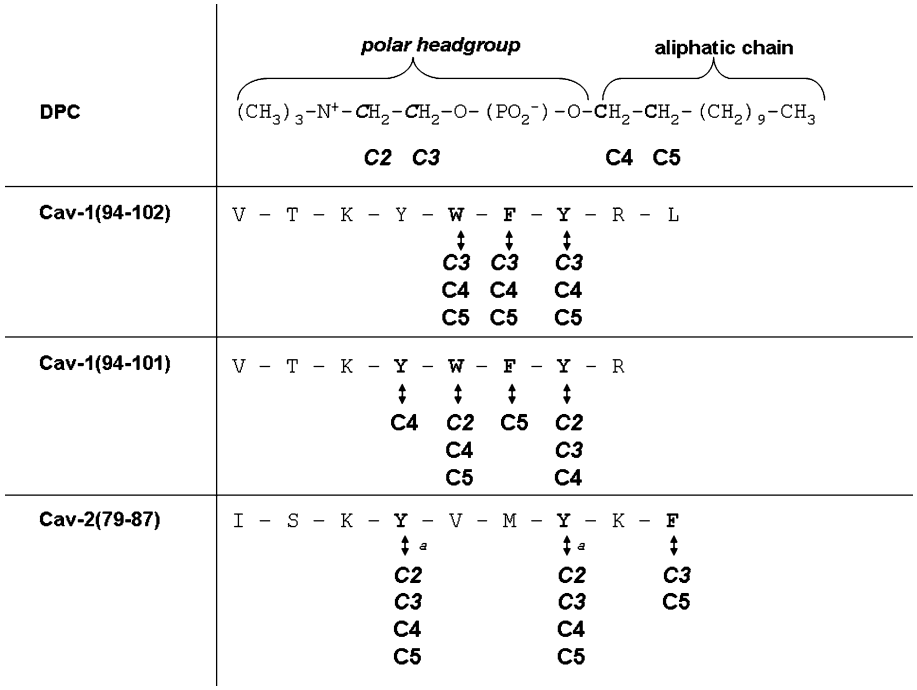

Fig. 9 Aromatic residues of cav-1(94–102), cav-1(94–101), and cav-2(79–87) peptides involved in NOEs with DPC methylene protons. Aromatic residues are shown in *bold*. The methylene protons of the polar head group of DPC are shown in *bold italic* and the aliphatic chain protons of DPC are shown in **bold** typeface. *a* corresponds to the resonance overlap between $H^{\varepsilon 1/\varepsilon 2}$ of Y82 and $H^{\varepsilon 1/\varepsilon 2}$ of Y85 of cav-2(79–87)

for cav-1(94–102). A long series of large positive $^{13}C_\alpha$ chemical shift indices ($\Delta\delta C_\alpha$) was observed for all but the last two residues (Fig. 7a). The presence of a large number of intense ($i, i + 3$) NOEs (Fig. 7b, middle panel) indicated that the peptide adopted a helical conformation from I79 to K87. Indeed, the $^{13}C_\alpha$ chemical shift indices for residues 79–85 were particularly large (up to 4 ppm), and larger than those obtained for cav-1(94–102). These results suggest that cav-2(79–87) has a more stable helical conformation than cav-1(94–102). In addition, dNN ($i, i + 3$) NOEs connectivities were observed only for cav-2(79–87), and dαN ($i, i + 3$) NOEs were also more intense for this peptide.

We compared the localization of the cav-2(79–87) and cav-1(94–102) peptides in DPC micelles by analyzing intermolecular NOEs with the DPC signal (Fig. 9 and Table 1 of the Supplementary Material). For this purpose, NOESY spectra of the peptides solubilized in deuterated DPC micelles were compared in the presence and absence of protonated DPC (10%) in D_2O. Unfortunately, the intense signals of protonated DPC made the reliable observation of intermolecular NOEs between protonated DPC and the aliphatic protons of the peptide impossible. However, many intermolecular NOEs between the DPC methylene protons on either side of the anionic phosphate group and peptide aromatic protons could be observed (see Fig. 9 and Table 1 of the Supplementary Material). All aromatic protons of cav-1(94–102) other than Y97, W98, F99, and Y100 gave rise to intermolecular NOEs with DPC signals corresponding to the C3, C4, C5 methylene protons, but not the C2 methylene protons.

In addition, intermolecular NOEs between the aromatic residues of cav-2(79–87) Y82 and/or Y85 and F87 and the C2, C3, C4, C5 DPC methylene protons were observed. The intermolecular NOEs observed between the tyrosine aromatic protons and DPC methylene protons remained ambiguous due to resonance overlaps involving the aromatic protons of Y82 and Y85.

The intermolecular NOEs therefore indicate that both peptides—cav-1(94–102) and cav-2(79–87)—are located in the polar head group region of the DPC micelles, encompassing the first two methylene groups of the DPC acyl chain.

NMR comparison of the structural properties of cav-1(94–101) and cav-1(94–102)

Finally, we investigated the role of the C-terminal hydrophobic residue in the structure and membrane attachment of the cav-1(94–102) peptide by studying the structural properties of the shorter CRAC motif—the cav-1(94–101) octapeptide. This motif displayed a lower level of binding to DPC micelles, as shown by the higher DPC concentration required to obtain a plateau region in titration curves of proton chemical shifts as a function of DPC concentration [100 mM for cav-1(94–102) and 400 mM for cav-1(94–101); data not shown]. A series of positive $^{13}C_\alpha$ chemical shift differences between observed and random coil values exceeding 0.7 ppm was observed for residues Val94 to Trp98 (Fig. 7a). The three C-terminal residues Phe99 to R101 had a smaller $\Delta\delta C_\alpha$ than the N-terminal residues. The presence of dαβ ($i, i + 3$) NOEs involving

residues V94 to Y97 and dαN (i, $i + 4$) connectivities (Fig. 7b) between V94 and W98 residues indicates that only segment V94 to W98 (i.e., five amino acids) adopts a stable helical conformation, consistent with $\Delta\delta C_\alpha$ values (see Fig. 7a). However, the presence of a large number of intense (i, $i + 3$) NOEs and the greater value of the $^{13}C_\alpha$ chemical shift difference obtained for the cav-1(94–102) nonapeptide than for the octapeptide indicated that the octapeptide was less structured than the nonapeptide.

We compared the accessibility to solvent of the amide backbone protons of the two cav-1 peptides by carrying out proton/deuterium exchange experiments. All the amides of the shorter peptide exchanged rapidly within the dead time of the experiment, i.e., within 5 min, whereas for the slowest exchanging amide proton of Phe99 of cav-1, the exchange occurred within 20 min. These results suggest that the shorter cav-1 peptide does not form particularly stable intra- or intermolecule hydrogen bonds.

For the localization of cav-1(94–101) within DPC micelles, we analyzed intermolecular NOEs with the DPC signals (Fig. 9 and Table 1 of the Supplementary Material). Intermolecular NOE cross peaks were observed between Y100 aromatic protons and the DPC proton signals of the C2, C3, and C4 methylene groups. In addition, intermolecular NOE cross peaks including the Y97 and F99 aromatic protons were observed only with the DPC proton signals of the C4 and C5 methylene groups, respectively. It therefore seems that cav-1(94–101), like cav-1(94–102), is located in the polar head group region of DPC micelles.

Discussion

This paper describes the detailed structural and dynamic characterization, in membrane mimics, of three juxtamembrane caveolin segments located upstream from the hydrophobic domain: two cav-1 peptides encompassing the CRAC motif (V94-T-K-Y-W-F-Y-R-L102 and V94-T-K-Y-W-F-Y-R101) and a homologous cav-2 peptide (I79-S-K-Y-V-M-Y-K-F87). In this study, we combined several complementary spectroscopic techniques to follow peptide binding to membrane mimics and the resulting changes in the molecular properties of the peptide.

Partitioning of cav-1(94–102), cav-1(94–101), and cav-2(79–87) into various membrane models

The two positive charges on cav-1(94–102) make it readily soluble in buffer, where it is largely unstructured, as shown by CD and NMR spectroscopy. In this state, the single tryptophan residue, W98, is largely accessible to bulk water, as shown by its fluorescence spectrum, characterized by a single component with $\lambda_{max} = 347$ nm and its almost complete accessibility to acrylamide (90%, using NATA as a reference). Furthermore, taking into account the Perrin equation (see "Materials and methods"; Perrin 1936) and reference data with various proteins (Gallay et al. 2004), the W98 subnanosecond rotational correlation time obtained from time-resolved fluorescence anisotropy measurements indicated an absence of aggregation.

The interaction of cav-1(94–102) with detergent micelles was followed by studying changes in various properties of the peptide (W98 fluorescence characteristics and ^1H chemical shift variations) and searching for direct evidence of peptide-detergent contact (by NOE interaction, for example). The plateau regions obtained in the fluorescence and NMR titration curves of cav-1(94–102) with DPC revealed that this peptide was readily completely partitioned into DPC micelles. In addition, intermolecular NOEs provided evidence that several methylene protons on either side of the DPC phosphate group were located close to the aromatic protons of the peptide. Fluorescence titration by DM also showed that cav-1(94–102) partitioned into these detergent micelles but to a lesser extent than into DPC micelles. In DM micelles, peptide–detergent interaction was also directly demonstrated by the fluorescence quenching of W98 by two brominated detergents (BrUM or BrDM), as a quenching of this type (a heavy-atom quenching) requires "contact" between bromine atoms and the indole ring.

In the presence of DM or DPC micelles, the longest Trp rotational correlation time (θ) provides information about the Brownian motion of the peptide-detergent complexes. These complexes were similar in size to the corresponding pure micelles, according to the θ values (10–15 ns). They probably contained no more than one peptide per complex because of the experimental conditions used (slight excess of micelles over peptide) and the electrostatic repulsion between these cationic peptides.

The weaker peptide partitioning in DM than in DPC micelles led us to investigate whether specific lipid–peptide interactions may be demonstrated using the former system. Such specific interaction might play a role in lipid segregation occurring in caveolae.

The modulation of peptide partitioning into mixed micelles of DM enriched with a small amount (10%, mol/mol) of various neutral and anionic phospholipids failed to indicate specific interactions but highlighted the dominant effect of electrostatic interactions.

The absence of an effect of doping DM micelles with 10% DMPC indicates that electrostatic interactions between the peptide and the zwitterionic phosphocholine group (common to DMPC and DPC) cannot account for the major difference between the peptide titration curves obtained with DM and DPC. The difference in the ability of these two types of detergent micelles to accommodate

the peptide is probably related to the chemical nature of their polar head groups, conferring specific structural and dynamic properties on their micelle-water interfaces and on the detergent monomers in the micelles (Dupuy et al. 1997; Tieleman et al. 2000). DM micelles have been shown to have an H-bond network between the OH groups of the interfacially located sugar moieties and hydration water (Drummond et al. 1985), rendering the hydrated maltose moiety noninteractive (Warr et al. 1986). The polar head group region of zwitterionic DPC micelles is in a less compact and more dynamic state than that of DM micelles (Tortech et al. 2001), increasing the likelihood that these peptides can be accommodated.

The importance of electrostatic interactions with negatively charged phospholipids in this study is consistent with the findings of McLaughlin et al. (Arbuzova et al. 2000) for the cav-1(92–101) peptide, which is one amino acid shorter and has two positive charges, like cav-1(94–102). They showed that POPS and POPG generated similar increases in the partitioning of the cav-1(92–101) peptide into large mixed POPS/POPC and POPG/POPC unilamellar vesicles over that observed with POPC alone.

Our titration data, analyzed in terms of a partition coefficient from water to a micellar phase, were compared with the thermodynamic data predicted on the basis of the peptide sequence. If an interfacial partitioning free energy (ΔG) from the Hristova and White scale (the most suitable scale for such an amphiphilic peptide) established with POPC as a lipid (Hristova and White 2005) is assigned to each amino acid, a ΔG value of -6.0 kcal/mol is obtained for the partitioning of the unstructured cav-1(94–102) peptide into a lipid interface, demonstrating the hydrophobic character of this sequence. In addition, each residue involved in an α helix structure may contribute about -0.4 kcal/mol to ΔG, as suggested by the MPEX site (http://blanco.biomol.uci.edu/mpex). Our NMR experiments showed cav-1(94–102) to be mostly helical, giving a final range of ΔG: $-9.6 < \Delta G < -8.8$ kcal/mol (assuming seven to nine helical residues, taking into account the fraying ends). In DPC micelles, an upper boundary for ΔG of -6.5 kcal/mol was calculated from the partition coefficient K (see "Materials and methods"). This difference in ΔG values may be accounted for by differences in the systems used and in the hypotheses underlying ΔG calculations (such as ΔG contribution for residues in an α helical conformation).

NMR showed that cav-1(94–102) and cav-2(79–87) gave similar titration curves with DPC. For cav-2, a ΔG value of -3.9 kcal/mol was obtained for the partitioning of the unstructured cav-2(79–87) peptide and a ΔG range of -6.7 to -7.5 kcal/mol was obtained taking peptide folding into account. The ability of both these peptides to adopt a helical structure and the hydrophobicity of their sequences seemed to make similar contributions to their free energy for membrane interaction.

For the cav-1(94–101) octapeptide, a higher DPC concentration (400 mM) was required for complete peptide partitioning, as shown by NMR titration. With the same method, we obtained ΔG values of -5.4 and -7.4 kcal/mol (assuming that five of eight residues are in helical conformation) for the unstructured and structured peptides, respectively. Consistent with the titration curve, these values indicate that this shorter peptide was less likely than the corresponding nonapeptide to partition within a membrane interface. These results are consistent with those of Epand et al. (2005), who observed little secondary structure for the same octapeptide in the presence of POPC and a higher λ_{max} of 339 nm for W98 than the 332 nm observed for the cav-1 nonapeptide.

Location of aromatic residues of cav-1(94–102) in DPC and DM micelles

Trp is a sensitive reporter of its immediate environment because its fluorescence spectrum is highly dependent on the polarity of its environment and on the presence of neighboring polar or charged groups (Chen and Barkley 1998; Lakowicz 1999; Vivian and Callis 2001). In addition, its fluorescence may be quenched highly efficiently by various compounds, such as the acrylamide and brominated compounds used here. For these two examples, collision or close contact is required for quenching, so fluorescence intensity provides information about the physical accessibility of Trp to these quenchers.

When complete partitioning of cav-1(94–102) into micelles was observed, as in 4 mM DPC or 6 mM DM-DMPS micelles, the strong blue-shift of the peptide fluorescence spectrum (15 and 20 nm, respectively, versus that in buffer), together with the significant decrease in W98 accessibility to acrylamide (accessibility estimated at $\sim$40% with respect to NATA) clearly indicated that this peptide was inserted into the micelles. Furthermore, the W98 residue was generally found in the polar head group region as shown by comparison of the λ_{max} value of cav-1(94–102) and the lattice parameter n of its quenching by brominated detergent with those obtained with six poly-Leu-type transmembrane model peptides P_n (e.g., P3: K2WL9AL9K2A), containing a single Trp at various positions in the sequence (de Foresta et al. 2002; Vincent et al. 2007).

However, a diversity of locations is suggested by the decomposition of the W98 fluorescence spectra in DM and DPC micelles into two spectral components. The decomposition is similar to that obtained for the model peptides P3, P5, and P7 in DPC, with a Trp residue located in the polar head group region (de Foresta et al. 2002).

These results are consistent with the W98 residue slowly exchanging (more slowly than over the nanosecond time scale) between two microenvironments. Although originally defined for Trp residues in proteins, the Burstein classification of Trp spectral properties as a function of the microenvironment may be extended to other macromolecular assemblies, such as membranes or micelles (Burstein et al. 2001; Reshetnyak and Burstein 2001). Thus, the fluorescence emission maximum at ~322–325 nm may correspond to a location at which the Trp residue can be H-bonded to very few water molecules (or other dipolar moieties). This location may correspond to the first methylene carbon region of the detergent acyl chain. The fluorescence emission maximum at ~342–344 nm may correspond to Trp in the highly hydrated polar head groups of each detergent, which contain slowly relaxing water molecules (Bhattacharyya and Bagchi 2000; Vincent et al. 2005). This location is consistent with the NOEs observed between W98 aromatic protons and methylene protons situated on either side of the anionic phosphate group of DPC. The shallow insertion of the peptide in the polar head group region of DPC micelles was also assessed by monitoring the intermolecular NOEs observed between methylene protons of the polar head of DPC and the other aromatic protons of the peptide. Limited rotations of the whole helix, with concomitant rearrangement of DPC molecules in the close vicinity of the peptide, may contribute to the heterogeneity of aromatic residue location and environment.

Bound cav-1(94–102) is structured as a stable helix

Cav-1(94–102) has a very low helical propensity [0.4% according to AGADIR software (Muñoz and Serrano 1995)] but forms a stable helix in the presence of DPC micelles, as demonstrated by CD and NMR experiments. This finding is consistent with our previous CD and NMR data for the longest peptide cav-1(82–109) (Le Lan et al. 2006). The presence of a predominantly helical conformation in DPC is also consistent with the appearance of a dominant long excited state lifetime for W98 (Willis et al. 1994). The helix is amphipathic, with the two tyrosine side chains flanked by the two charged arginine and lysine side chains on one face, and the phenylalanine and tryptophan side-chains on the other face. The helix is located in the polar head group region of the DPC micelle, as shown above. As shown by the molecular dynamics of the DPC micelle, the packing of the head group is quite loose (Wymore et al. 1999), allowing it to accomodate such a structure. The radius of the micelle is about 22 Å, with a polar head group thickness of ~4 Å [from the probability distribution of the first carbon of the acyl chain, referred to as C4 in this paper (Fig. 9), and the nitrogen atom] to ~9 Å if the hydration shell is taken into account (Tieleman et al. 2000). These dimensions are suitable for the incorporation of an α-helix with a backbone diameter of 4 Å.

Role of the various amino acids

The main difference between cav-1(94–102) and the homologous cav-2(79–87) sequence concerns the two central aromatic residues of the cav-1 sequence (WF), which are replaced by two aliphatic residues in cav-2 (VM). These peptides also differ for four other residues. They therefore also have different ΔG values for partitioning. They also differ in their hydrophobic moment μ, a parameter related to the periodicity in the polar/apolar character of a sequence (Eisenberg et al. 1984). Higher hydrophobic moments are correlated with higher asymmetry of the polar/apolar amino acid distribution around the helix axis (Eisenberg et al. 1984; Fernandez-Vidal et al. 2007; Phoenix et al. 2002). We obtained μ values of 1.53 and 0.33 for cav-1(94–102) and cav-2(79–87), respectively, with MPEX (Hristova and White 2005), for a helical conformation. These values are lower than those obtained for peptides with the same amino acid content but a different sequence (for cav-1, $\mu = 5.94$, for instance, for the sequence YYRTWVKLF; for cav-2, $\mu = 4.74$ for the sequence YIKVFSKMY). The hydrophobic moment of this amino acid sequence is therefore not optimized for membrane interaction. Going against expectations (Fernandez-Vidal et al. 2007), both the differences in chemical shift indices and in the NOEs observed for these two peptides indicate that cav-1(94–102), which has the highest hydrophobic moment, forms a less stable helix than cav-2(79–87).

Although few studies are devoted to caveolin-2, the main difference between caveolin-1 and caveolin-2 is related to the fact that caveolin-1 is essential for the formation of caveolae while this is not the case for caveolin-2. These differences could be linked to different abilities to make interactions with partners (proteins and/or lipids). The more flexible juxta-membrane sequence of cav-1 compared to cav-2 may facilitate the interactions with different partners as this region of cav-1 has been identified as part of an interaction domain with both lipids and proteins.

Both cav-1(94–102) and cav-2(79–87) are located in the polar head group region of DPC micelles. Differences were, however, observed in the intermolecular NOEs for these two peptides. These differences are difficult to interpret and may result from subtle differences in the degree of insertion, helix tilt, or the dynamic equilibrium of the peptide in the interface region.

By contrast, deletion of the C-terminal residue of cav-1(94–102)—L102—resulted in more extensive changes:

a lower level of structuration and weaker partitioning into DPC micelles. The calculated hydrophobic moment μ was also lower than that of the longer peptide (1.02 vs. 1.53). The properties of the shorter cav-1(95–101) have been studied by other groups (Sowmya et al. 2006; Woodman et al. 2002). Lisanti et al. (Woodman et al. 2002) showed that this amino acid sequence was sufficient for attachment of the soluble GFP protein to the membrane. This apparent discrepancy in affinity is probably due to the presence of charged phospholipids in biological membranes, which we showed to be important in our model system.

In conditions of complete binding, the weaker structuration and shallower insertion at the micellar interface of cav-1(94–101) than of cav-1(94–102) demonstrated by NMR thus highlights the importance played by the C-terminal hydrophobic residue L102 in both the structure and positioning of the peptide. However, the contributions of the partition enhancement and the stabilization of the helix cannot be precisely delineated.

Although we did not mutate the tyrosine residues, we suggest an essential role of the K/RhhhYR/Kh motif (h being a hydrophobic residue). The two charged residues are important for membrane binding and are conserved among caveolin homologs and sequences from different species. Tyr100 is also highly conserved. In addition, K96/Y100 cation-π interactions may contribute to helix stabilization, together with Y97/R101 interactions. Interchanging K and R does not affect the partitioning of the peptide in DPC and its helical secondary structure (data not shown).

The homologous cav-3 sequence (V67SKYWCYRL75) differs from that of cav-1 by two amino acid residues of similar hydrophobicity (T95 → S68, F99 → C72; Fig. 1). As a result, cav-3(67–75) has a hydrophobic moment similar to that of cav-1(94–102) ($\mu = 1.64$ and 1.53, respectively). Moreover, Thr95 is also replaced by Ser and Phe99 by Met in cav-2(79–87), resulting in only small changes, such that cav-3(67–75) probably also forms an amphipathic helix at the membrane interface.

Conclusion

We provide here a detailed characterization of the interaction of the cav-1(94–102) juxta-membrane segment with various membrane mimics. This segment includes a CRAC motif that may be important for the interaction of caveolin-1 with cellular membranes. Comparisons were made with the homologous sequence cav-2(79–87) and the shorter sequence cav-1(94–101), with the aim of determining the roles of particular amino acids in the interaction with membrane mimics. According to CD and NMR data, the cav-1(94–102) peptide was unfolded in water. Partitioning of the peptide in DPC or DM micelles was coupled with the formation of an amphipathic α-helix that, in DPC, was remarkably stable for such a short peptide. The limited availability of water molecules for the formation of intermolecular H-bonds with the peptide in the water/micelle interface favors the formation of intramolecular H-bonds stabilizing the helical folding of the peptide. The partitioning of this cationic peptide was stronger in DPC than in DM micelles. Partitioning in DM micelles was strongly enhanced by small amounts of anionic phospholipids, highlighting the role of electrostatic interactions favoring the anchoring of caveolin to the membrane. The free energy of α-helix formation may make a significant contribution to the interaction with DPC micelles. The detailed model obtained from NMR data shows the opposite positioning of charged R and K residues on one hand and W and F on the other hand. The helical peptide is located in an average shallow position, in the polar head group region of the micelle, as shown by fluorescence data and intermolecular NOEs, with the aromatic doublet W98-F99 probably pointing towards the inside of the micelle on average. However, this aromatic doublet is not essential for this interaction because cav-2(79–87), in which V83-M84 replaces W98-F99, displays similar partitioning in DPC and forms an even more stable helix. Similar behavior may also be predicted for the homologous cav-3(67–75), as its sequence differs only slightly from those of the other two peptides. The decision to study the cav-1 nonapeptide rather than the octapeptide proved judicious, as the octapeptide displayed weaker partitioning in DPC and was not completely structured even when bound to micelles. Our data thus reveal the role of L102 in stabilizing this interfacial helix. Finally, we suggest that the caveolin motif K/RhhhYR/Kh (h being a hydrophobic residue) plays an important role as a membrane interfacial anchor, based both on our results and the conservation of this motif in homologous sequences and between species.

Acknowledgments This paper is dedicated to the memory of J-M Neumann, who died during the course of this work.

References

Arbuzova A, Wang L, Wang J, Hangyas-Mihalyne G, Murray D, Honig B, McLaughlin S (2000) Membrane binding of peptides containing both basic and aromatic residues. Experimental studies with peptides corresponding to the scaffolding region of caveolin and the effector region of MARCKS. Biochemistry 39:10330–10339

Ben-Tal N, Honig B, Peitzsch RM, Denisov G, McLaughlin S (1996) Binding of small basic peptides to membranes containing acidic lipids: theoretical models and experimental results. Biophys J 71:561–575

Beswick V, Guerois R, Cordier-Ochsenbein F, Coïc YM, Tam HD, Tostain J, Noël JP, Sanson A, Neumann JM (1999)

Dodecylphosphocholine micelles as a membrane-like environment: new results from NMR relaxation and paramagnetic relaxation enhancement analysis. Eur Biophys J 28:48–58

Bhattacharyya K, Bagchi B (2000) Slow dynamics of constrained water in complex geometries. J Phys Chem A 104:10603–10613

Bocquet N, Nury H, Baaden M, Le Poupon C, Changeux JP, Delarue M, Corringer PJ (2009) X-ray structure of a pentameric ligand-gated ion channel in an apparently open conformation. Nature 457:111–114

Bouhss A, Vincent M, Munier H, Gilles AM, Takahashi M, Bârzu O, Danchin A, Gallay J (1996) Conformational transitions within the calmodulin-binding site of *Bordetella pertussis* adenylate cyclase studied by time-resolved fluorescence of Trp242 and circular dichroism. Eur J Biochem 237:619–628

Brochon JC (1994) Maximum entropy method of data analysis in time-resolved spectroscopy. Methods Enzymol 240:262–311

Brown LR, Bosch C, Wüthrich K (1981) Location and orientation relative to the micelle surface for glucagon in mixed micelles with dodecylphosphocholine: EPR and NMR studies. Biochim Biophys Acta 642:296–312

Burstein EA, Emelyanenko VI (1996) Log-normal description of fluorescence spectra of organic fluorophores. Photochem Photobiol 64:316–320

Burstein EA, Abornev SM, Reshetnyak YK (2001) Decomposition of protein tryptophan fluorescence spectra into log-normal components. I. Decomposition algorithms. Biophys J 81:1699–1709

Chen Y, Barkley MD (1998) Toward understanding tryptophan fluorescence in proteins. Biochemistry 37:9976–9982

Cohen AW, Hnasko R, Schubert W, Lisanti MP (2004) Role of caveolae and caveolins in health and disease. Physiol Rev 84:1341–1379

Coïc YM, Vincent M, Gallay J, Baleux F, Mousson F, Beswick V, Neumann JM, de Foresta B (2005) Single-spanning membrane protein insertion in membrane mimetic systems: role and localization of aromatic residues. Eur Biophys J 35:27–39

de Foresta B, Legros N, Plusquellec D, Le Maire M, Champeil P (1996) Brominated detergents as tools to study protein–detergent interactions. Eur J Biochem 241:343–354

de Foresta B, Gallay J, Sopkova J, Champeil P, Vincent M (1999) Tryptophan octyl ester in detergent micelles of dodecylmaltoside: fluorescence properties and quenching by brominated detergent analogs. Biophys J 77:3071–3084

de Foresta B, Tortech L, Vincent M, Gallay J (2002) Location and dynamics of tryptophan in transmembrane alpha-helix peptides: a fluorescence and circular dichroism study. Eur Biophys J 31:185–197

Drummond CJ, Warr GG, Grieser F, Ninham BW, Fennell Evans D (1985) Surface properties and micellar interfacial microenvironment of *n*-dodecyl-β-D-maltoside. J Phys Chem 89:2103–2109

Dupuy C, Auvray X, Petipas C, Rico-Lattes I, Lattes A (1997) Anomeric effects on the structure of micelles of alkyl maltosides in water. Langmuir 13:3965–3967

East JM, Lee AG (1982) Lipid selectivity of the calcium and magnesium ion dependent adenosinetriphosphatase, studied with fluorescence quenching by a brominated phospholipid. Biochemistry 21:4144–4151

Eftink MR (1991) Fluorescence techniques for studying protein structure. Methods Biochem Anal 35:127–205

Eisenberg D, Weiss RM, Terwilliger TC (1984) The hydrophobic moment detects periodicity in protein hydrophobicity. Proc Natl Acad Sci USA 81:140–144

Epand RM, Sayer BG, Epand RF (2003) Peptide-induced formation of cholesterol-rich domains. Biochemistry 42:14677–14689

Epand RM, Sayer BG, Epand RF (2005) Caveolin scaffolding region and cholesterol-rich domains in membranes. J Mol Biol 345:339–350

Fernandez-Vidal M, Jayasinghe S, Ladokhin AS, White SH (2007) Folding amphipathic helices into membranes: amphiphilicity trumps hydrophobicity. J Mol Biol 370:459–470

Gallay J, Vincent M, de la Sierra IML, Munier-Lehmann H, Renouard M, Sakamoto H, Barzu O, Gilles AM (2004) Insight into the activation mechanism of *Bordetella pertussis* adenylate cyclase by calmodulin using fluorescence spectroscopy. Eur J Biochem 271:821–833

Hristova K, White SH (2005) An experiment-based algorithm for predicting the partitioning of unfolded peptides into phosphatidylcholine bilayer interfaces. Biochemistry 44:12614–12619

Krittanai C, Johnson WC (1997) Correcting the circular dichroism spectra of peptides for contributions of absorbing side chains. Anal Biochem 253:57–64

Lakowicz JR (1999) Principles of fluorescence spectroscopy. Kluwer, New York

Lauterwein J, Bösch C, Brown LR, Wüthrich K (1979) Physicochemical studies of the protein–lipid interactions in melittin-containing micelles. Biochim Biophys Acta 556:244–264

Le Lan C, Neumann JM, Jamin N (2006) Role of the membrane interface on the conformation of the caveolin scaffolding domain: a CD and NMR study. FEBS Lett 580:5301–5305

le Maire M, Champeil P, Møller JV (2000) Interaction of membrane proteins and lipids with solubilizing detergents. Biochim Biophys Acta 1508:86–111

Li H, Papadopoulos V (1998) Peripheral-type benzodiazepine receptor function in cholesterol transport. Identification of a putative cholesterol recognition/interaction amino acid sequence and consensus pattern. Endocrinology 139:4991–4997

Liu P, Rudick M, Anderson RG (2002) Multiple functions of caveolin-1. J Biol Chem 277:41295–41298

Livesey AK, Brochon JC (1987) Analyzing the distribution of decay constants in pulse-fluorimetry using the maximum entropy method. Biophys J 52:693–706

London E, Feigenson GW (1981) Fluorescence quenching in model membranes. 2. Determination of local lipid environment of the calcium adenosinetriphosphatase from sarcoplasmic reticulum. Biochemistry 20:1939–1948

Lund S, Orlowski S, de Foresta B, Champeil P, le Maire M, Møller JV (1989) Detergent structure and associated lipid as determinants in the stabilization of solubilized Ca^{2+}-ATPase from sarcoplasmic reticulum. J Biol Chem 264:4907–4915

Moors SL, Hellings M, De Maeyer M, Engelborghs Y, Ceulemans A (2006) Tryptophan rotamers as evidenced by X-ray, fluorescence lifetimes, and molecular dynamics modeling. Biophys J 91:816–823

Muñoz V, Serrano L (1995) Elucidating the folding problem of helical peptides using empirical parameters. II. Helix macrodipole effects and rational modification of the helical content of natural peptides. J Mol Biol 245:275–296

Murray D, Hermida-Matsumoto L, Buser CA, Tsang J, Sigal CT, Ben-Tal N, Honig B, Resh MD, McLaughlin S (1998) Electrostatics and the membrane association of Src: theory and experiment. Biochemistry 37:2145–2159

Nanga RP, Brender JR, Xu J, Veglia G, Ramamoorthy A (2008) Structures of rat and human islet amyloid polypeptide IAPP1–19 in micelles by NMR spectroscopy. Biochemistry 47:12689–12697

Neumoin A, Arshava B, Becker J, Zerbe O, Naider F (2007) NMR studies in dodecylphosphocholine of a fragment containing the seventh transmembrane helix of a G-protein-coupled receptor from *Saccharomyces cerevisiae*. Biophys J 93:467–482

Pace CN, Vajdos F, Fee L, Grimsley G, Gray T (1995) How to measure and predict the molar absorption coefficient of a protein. Protein Sci 4:2411–2423

Pan CP, Barkley MD (2004) Conformational effects on tryptophan fluorescence in cyclic hexapeptides. Biophys J 86:3828–3835

Parton RG, Simons K (2007) The multiple faces of caveolae. Nat Rev Mol Cell Biol 8:185–194

Parton RG, Hanzal-Bayer M, Hancock JF (2006) Biogenesis of caveolae: a structural model for caveolin-induced domain formation. J Cell Sci 119:787–796

Peitzsch RM, McLaughlin S (1993) Binding of acylated peptides and fatty acids to phospholipid vesicles: pertinence to myristoylated proteins. Biochemistry 32:10436–10443

Perrin F (1936) Mouvement brownien d'un ellipsoide (II). Rotation libre et dépolarisation des fluorescences. Translation et diffusion de molécules ellipsoidales. J Phys et le Radium 7:1–11

Phoenix DA, Harris F, Daman OA, Wallace J (2002) The prediction of amphiphilic alpha-helices. Curr Protein Pept Sci 3:201–221

Powl AM, East JM, Lee AG (2005) Heterogeneity in the binding of lipid molecules to the surface of a membrane protein: hot spots for anionic lipids on the mechanosensitive channel of large conductance MscL and effects on conformation. Biochemistry 44:5873–5883

Reshetnyak YK, Burstein EA (2001) Decomposition of protein tryptophan fluorescence spectra into log-normal components. II. The statistical proof of discreteness of tryptophan classes in proteins. Biophys J 81:1710–1734

Roche S, Bressanelli S, Rey FA, Gaudin Y (2006) Crystal structure of the low-pH form of the vesicular stomatitis virus glycoprotein G. Science 313:187–191

Rogers DM, Hirst JD (2004) First-principles calculations of protein circular dichroism in the near ultraviolet. Biochemistry 43:11092–11102

Rosevear P, VanAken T, Baxter J, Ferguson-Miller S (1980) Alkyl glycoside detergents: a simpler synthesis and their effects on kinetic and physical properties of cytochrome *c* oxidase. Biochemistry 19:4108–4115

Rouvière N, Vincent M, Craescu CT, Gallay J (1997) Immunosuppressor binding to the immunophilin FKBP59 affects the local structural dynamics of a surface beta-strand: time-resolved fluorescence study. Biochemistry 36:7339–7352

Santos NC, Prieto M, Castanho MA (2003) Quantifying molecular partition into model systems of biomembranes: an emphasis on optical spectroscopic methods. Biochim Biophys Acta 1612: 123–135

Schibli DJ, Nguyen LT, Kernaghan SD, Rekdal O, Vogel HJ (2006) Structure–function analysis of tritrpticin analogs: potential relationships between antimicrobial activities, model membrane interactions, and their micelle-bound NMR structures. Biophys J 91:4413–4426

Schlegel A, Schwab RB, Scherer PE, Lisanti MP (1999) A role for the caveolin scaffolding domain in mediating the membrane attachment of caveolin-1. The caveolin scaffolding domain is both necessary and sufficient for membrane binding in vitro. J Biol Chem 274:22660–22667

Seelig J (2004) Thermodynamics of lipid-peptide interactions. Biochim Biophys Acta 1666:40–50

Sillen A, Engelborghs Y (1998) The correct use of "average" fluorescence parameters. Photochem Photobiol 67:475–486

Sjögren H, Ericsson CA, Evenas J, Ulvenlund S (2005) Interactions between charged polypeptides and nonionic surfactants. Biophys J 89:4219–4233

Sowmya BL, Jagannadham MV, Nagaraj R (2006) Interaction of synthetic peptides corresponding to the scaffolding domain of caveolin-3 with model membranes. Biopolymers 84:615–624

Tamm LK (1991) Membrane insertion and lateral mobility of synthetic amphiphilic signal peptides in lipid model membranes. Biochim Biophys Acta 1071:123–148

Tieleman DP, van der Spoel D, Berendsen HJC (2000) Molecular dynamics simulations of dodecylphosphocholine micelles at three different aggregate sizes: micellar structure and chain relaxation. J Phys Chem B 104:6380–6388

Tortech L, Jaxel C, Vincent M, Gallay J, de Foresta B (2001) The polar headgroup of the detergent governs the accessibility to water of tryptophan octyl ester in host micelles. Biochim Biophys Acta 1514:76–86

Vincent M, Gallay J (1995) Solvent relaxation around the excited state of indole: analysis of fluorescence lifetime distributions and time-dependence spectral shifts. J Phys Chem 99:14931–14941

Vincent M, de Foresta B, Gallay J (2005) Nanosecond dynamics of a mimicked membrane-water interface observed by time-resolved stokes shift of LAURDAN. Biophys J 88:4337–4350

Vincent M, Gallay J, Jamin N, Garrigos M, de Foresta B (2007) The predicted transmembrane fragment 17 of the human multidrug resistance protein 1 (MRP1) behaves as an interfacial helix in membrane mimics. Biochim Biophys Acta 1768:538–552

Vivian JT, Callis PR (2001) Mechanisms of tryptophan fluorescence shifts in proteins. Biophys J 80:2093–2109

Warr GG, Drummond CJ, Grieser F, Ninham BW, Fennell Evans D (1986) Aqueous solution properties of nonionic *n*-dodecyl-*β*-D-maltoside micelles. J Phys Chem 90:4581–4586

Willis KJ, Neugebauer W, Sikorska M, Szabo AG (1994) Probing alpha-helical secondary structure at a specific site in model peptides via restriction of tryptophan side-chain rotamer conformation. Biophys J 66:1623–1630

Wimmer R, Andersen KK, Vad B, Davidsen M, Molgaard S, Nesgaard LW, Kristensen HH, Otzen DE (2006) Versatile interactions of the antimicrobial peptide novispirin with detergents and lipids. Biochemistry 45:481–497

Wishart DS, Bigam CG, Yao J, Abildgaard F, Dyson HJ, Oldfield E, Markley JL, Sykes BD (1995) ^{1}H, ^{13}C and ^{15}N chemical shift referencing in biomolecular NMR. J Biomol NMR 6:135–140

Woodman SE, Schlegel A, Cohen AW, Lisanti MP (2002) Mutational analysis identifies a short atypical membrane attachment sequence (KYWFYR) within caveolin-1. Biochemistry 41:3790–3795

Wüthrich K (1986) NMR of proteins and nucleic acids. John Wiley, New York

Wymore T, Gao XF, Wong T (1999) Molecular dynamics simulation of the structure and dynamics of a dodecylphosphocholine micelle in aqueous solution. J Mol Struct 485–486:195–210

Zhang Q, Horst R, Geralt M, Ma X, Hong WX, Finn MG, Stevens RC, Wüthrich K (2008) Microscale NMR screening of new detergents for membrane protein structural biology. J Am Chem Soc 130:7357–7363